Application of Magnesium Oxide Nanoparticles for Sunset Yellow Removal in Aqueous Solutions: Adsorption Isotherm, Kinetic, and Thermodynamic Studies

Marzbani, Tayebeh; Khayatian*+, Gholamreza

Department of Chemistry, Faculty of Sciences, University of Kurdistan, Sanandaj, I.R. IRAN

ABSTRACT: *In this research, the ability of magnesium oxide (MgO) nanoparticles to the adsorbent was studied for the removal of Sunset Yellow (SY) dye in an aqueous solution. Different techniques, including Fourier Transform InfraRed (FT-IR) spectroscopy and Scanning Electron Microscopy (SEM) were employed to identify the adsorbed dye. Adsorption experiments were carried out in a batch mode with varying pHs, MgO concentrations, initial dye concentrations, contact times, and temperatures. To study SY adsorption's efficiency on the surface of MgO nanoparticles, pseudo-first-order, second-order, and intra-particle diffusion kinetic models were investigated. The pseudo-second-order kinetic model demonstrated a better fitting than other kinetic models (correlation coefficient: R^2=0.99). The Freundlich model with an R^2=0.93 value proved to fit with equilibrium data. In addition, thermodynamic parameters consisting of enthalpy, entropy, and activation energy were calculated too. It was noticed that the adsorption of SY on MgO was exothermic and spontaneous at low temperatures. The suggested adsorbent can be utilized for removing SY with an efficiency of more than 85%.*

KEYWORDS: *Nanoparticle; Removal of sunset yellow; Isotherm; Kinetic and thermodynamic studies.*

INTRODUCTION

Different industrial processes such as paper-producing factories, dyeing plants, textile mills, and ink or paint producers use large amounts of dyes. Due to the stability of dyes and preventing the passage of light in the rivers, it is challenging to decolorize dye-containing wastewaters. Hence, it is essential to find more accessible and less costly procedures for removing dyes from industrial dye-containing wastewaters [1, 2]. The existence of dyes in waters leads to the emergence of environmental problems such as the loss of photosynthetic activity of aquatic plants because of less light penetration [3–5]. Therefore, the concentration of the dyes must be controlled because they are potentially harmful to humans [6].

Sunset yellow (SY) is an anionic dye with aromatic rings and an azo (N=N) functional group [7]. It is used in foodstuffs such as juices, candies, soft drinks, jellies, and salty snacks to give them yellow-orange coloring [8]. Furthermore, adding SY gives several improvements like high stability to oxygen, color uniformity, relatively low microbiological contamination, and lower production costs in drinks, food, or pharmaceutical preparations [9]. However, SY may bring about several side effects such as

* *To whom correspondence should be addressed.*
+E-mail address: gkhayatian@uok.ac.ir
1021-9986/2022/12/3939-3949 11/$/6.01

,

diarrhea, kidney tumors, hyperactivity, abdominal pain, nasal congestion, chromosomal damage, severe weight loss, and allergies [10]. Thus, despite their important role in our food, azo dyes could be a serious threat to human health. The Sunset Yellow was banned or restricted around the year 2000 as a food additive in many European countries, but still, it is used in Iran [11]. Most environmental pollutants due to human activity and industrial performance enter wastewaters. These pollutants get in the food chain and create a severe menace to humans. Hence, as an exciting research subject, their removal is vital in order to lessen their dangers. Different technologies have been adopted based on various principles such as physical, chemical, and biological to remove SY dye from wastewaters. In this regard, enzymatic techniques, coagulation, ozonation, photo-degradation, reverse osmosis, electrochemical oxidation, bio-sorption, and adsorption are efficiently used [12–14]. However, the adsorption process is the most commonly used technique. Because the adsorbents are readily available, their non-toxicity, high capacity and efficiency, and its potential for adsorbent regeneration can keep the quality of water intact in comparison to conventional methods of wastewater treatment, and nanoparticles are attracting a lot of attention day by day with their applications in different fields [15, 16].

This research work deals with the application of magnesium MgO as adsorbents of SY from an aqueous solution. Based on the unique properties of MgO, the MgONPs component are very important when compared with bulk materials. They possess outstanding properties such as high photocatalytic activity, chemical stability, electrical permittivity, heat resistance, non-toxicity [17, 18] low refractive index, and low dielectric constant, which has led to widespread applications in the fields of catalysis, paint, and semiconductor products and adsorption [19]. Moreover, they are readily available, non-volatile, low-cost, reusable, and have high adsorption capacity and high reactivity. In addition, since they have efficient adsorption capability, MgO nanoparticles can be employed in various fields such as ceramics, electronics, petrochemical products, and coatings catalysis. The intrinsic properties such as porous structure, high specific surface area, and enhanced surface binding sites enable MgO to perform well as an effective adsorbent in the remediation of contaminants from wastewater [20].

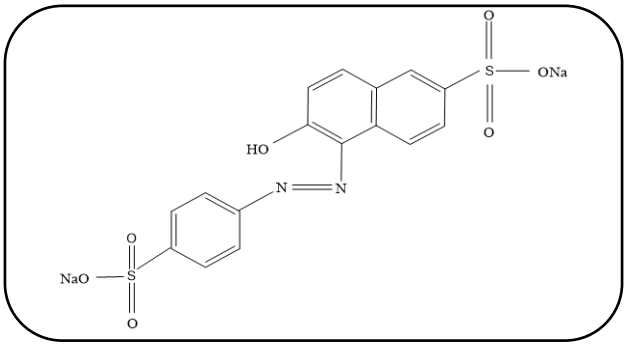

Fig. 1: Chemical structure of SY

This study's important aim is to conduct detailed adsorption research to eliminate SY by utilizing magnesium oxide nanoparticles (MgO). The different parameters were measured such as kinetic, isothermal, and thermodynamic studies. Other parameters such as pH, primary concentration, time, adsorbent dose, and temperature, which were involved in SY adsorption, were also studied.

EXPERIMENTAL SECTION

Reagents

The SY, HCl, and NaOH were purchased from Sigma Aldrich and Merck Company (Germany), respectively. The MgO nanoparticle was purchased from Kimia Rahavard Company, IRAN. The chemical structure of SY is shown in Fig. 1.

Preparation of Aqueous Dye Solutions

The commercial grade of SY dye was used as received. The dye stock solution (80 mg⁄ L) was prepared by dissolving 0.02 g of dye in 250 mL of distilled water. The different solution with various initial concentrations was prepared by diluting the SY dye stock solution (4.0 to 80.0 mg⁄L). The NaOH or HCl (0.1 M) was used to adjust the solutions' pH. The pH measurements were conducted by using pH meter model-691 (Metrohm, Swiss) with a combined glass electrode.

Characterization

The dye adsorbed on the MgO was dried under a vacuum at 80 °C for 4 h before being analyzed by FT-IR (Vector 22, German). Using FT-IR spectroscopy in the range of 500-4000 cm^{-1}, the adsorption peaks of SY, magnesium oxide (MgO) nanoparticles, and SY/MgO were obtained. Scanning electron microscopy (FE-SEM, ZEISS,

and SIGMA VP) was utilized to study the adsorbent's surface morphologies.

Adsorption studies

Batch-type adsorption was carried out using SY solutions (10.0 mL) in a 50 mL beaker with a known amount of adsorbent at a constant speed of 750 rpm. The effects of several variables on the adsorption; such as temperature (298–346K), contact time (5.0–100.0 min), pH (1.0–11.0), adsorbent dosage (1.0–15.0 mg), and dye concentration (4.0-80.0 mg⁄L) were also studied, and optimum values were evaluated. The UV-Vis spectrophotometer at a wavelength of 483 nm was used to determine SY concentrations before and after adsorption. The percentage of dye removal was measured by using the following equation:

$$\%R = \left(\frac{C_0 - C_e}{C_0}\right) \times 100 \quad (1)$$

In this formula, the C_e (mg⁄L) and C_0 (mg⁄L) are the equilibrium and initial concentrations of dye in the experimental solution, respectively. The following equation was used to calculate the equilibrium capacity of MgO adsorption:

The capacity of equilibrium adsorption was calculated from the following equation:

$$q_e = \frac{(C_0 - C_e)V}{w} \quad (2)$$

That q_e (mg⁄g) is the equilibrium adsorption capacity, V (L) is the volume of solution, C_e (mg⁄L) and C_0 (mg⁄L) are the equilibrium and initial concentrations of dye in the experimental solution, respectively and W (g) is the mass of the adsorbent.

Adsorption thermodynamic

Thermodynamics gives a vast amount of information on enthalpy (ΔH°) and entropy (ΔS°) changes in an adsorption process. The following equations were used to determine the thermodynamic parameters [21]:

$$Ln(K) = \frac{\Delta S^\bullet}{R} - \frac{\Delta H^\bullet}{RT} \quad (3)$$

$$K = \frac{q_e}{C_e} \quad (4)$$

With regard to thermodynamic data, Gibbs free energy ($\Delta G^\bullet$) is obtained from the following equation:

$$\Delta G^\bullet = \Delta H^\bullet - T\Delta S^\bullet \quad (5)$$

R is the Universal Gas constant; *K* depicts the balance constant and *T*(K) illustrates the temperature.

Adsorption isotherms

A quantitative relationship between the adsorbent surface and the amount of adsorption is required to study the adsorption process. These quantitative relationships are defined as the adsorption isotherms of Langmuir (Eq. (6)), Freundlich (Eq. (7)), and Temkin (Eq. (8)). Adsorption studies was utilized at different SY concentrations at constant pH, adsorbent amount, time, and temperature to investigate isotherm models.

The Langmuir isotherm equation is as follow [22]:

$$\frac{C_e}{q_e} = \frac{C_e}{q_m} + \frac{1}{(K_L \times q_m)} \quad (6)$$

q_e and q_m (mg⁄g) are the equilibrium and maximum adsorption capacity, respectively. C_e (mg⁄ L) show the equilibrium concentration of dye. K_L (L⁄ mg) is the Langmuir constant.

The Freundlich isotherm equation is as follows:

$$Lnq_e = LnK_F + \left(\frac{1}{n}\right) LnC_e \quad (7)$$

In this formula for the best and favorable adsorption process, n should be 1.0 <n<10.0. For n>10 (smaller value of 1/n) shows the higher adsorption intensity. For n=1, identical adsorption energies occur in all sites due to the linear adsorption process [23, 24].

q_e (mg⁄g) is the equilibrium adsorption capacity, C_e (mg⁄L) show the equilibrium concentration of dye, K_F (mg⁄g) depicts Freundlich adsorption capacity and in addition, n illustrates Freundlich constant

The Temkin isotherm equation is as follow [25]:

$$q_e = \mathrm{BLnA} + \mathrm{BLn}C_e \quad (8)$$

q_e (mg⁄g) is the equilibrium adsorption capacity, C_e (mg⁄L) show the equilibrium concentration of dye, *A* (L⁄g) represents Temkin constant and *B* (J⁄ mg) is Temkin's adsorption heat.

The basic properties of the Langmuir isotherm can be defines as a dimensionless constant R_L (Eq. (9)), is separation factor or equilibrium parameter as follows:

$$R_L = \frac{1}{\left(1 + (K_L \times C_0)\right)} \quad (9)$$

,

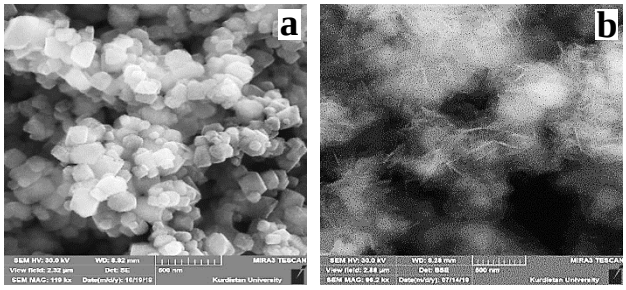

Fig. 2: SEM images of (a) MgO nanoparticle (b) MgO with adsorbed SY

$R_L > 1$, the reaction is unfavorable
$0 < R_L < 1$, it is favorable reaction
$R_L = 1$, the reaction is linear
$R_L = 0$ indicates an irreversible reaction
C_0 (mg/L) show the initial concentration, K_L (L/mg) is the Langmuir constant.

Adsorption kinetics

Kinetic models are among the most critical properties in determining adsorption efficiency. Various kinetic models have been offered in different studies. In this research, the following kinetic models were applied to analytical data. The pseudo-first-order and second-order (Eqs. (10) and (11), as well as Intra-particle diffusion (Eq. (12)) models, shows as following equations [26]:

The pseudo-first-order equation is as follows:

$$Ln(q_e - q_t) = Lnq_e - K_1 t \qquad (10)$$

The pseudo-second-order equation is as follows:

$$\frac{t}{q_t} = \frac{1}{(k_2 q_e^2) + \frac{t}{q_e}} \qquad (11)$$

The model of intra-particle diffusion is as follows:

$$q_t = K_p t^{1/2} + c \qquad (12)$$

q_t and q_e (mg/ g) are the adsorption capacity and equilibrium adsorption capacity at time *t*. k_1 (L/ min), k_2 (g/ mg.min) and k_p (mg/ gmin$^{1/2}$) represents the rate constant for pseudo-first-order, pseudo-second-order and intra-particle diffusion, respectively. In addition, C refers to constant boundary layer thickness.

RESULTS AND DISCUSSION

SEM analysis

A scanning electron microscope (SEM) is a very suitable tool for identifying the morphology of the adsorbent surface and the study of its physical properties to identify the shape and size of particles and the distribution of cavities. The surface morphology and the composition of MgO nanoparticles before and after SY adsorption are determined using an SEM instrument. The SEM micrographs show crystallites formation in different magnifications (including 500 nm). The MgO powder micrograph clearly illustrates the formation of the nanoparticles (Fig. 2a) with various morphology, like a cube in a high amount of agglomeration, after adsorption, the SEM images of MgO nanoparticles revealed that the MgO nanoparticles' surface was covered entirely with SY molecules (Fig. 2b).

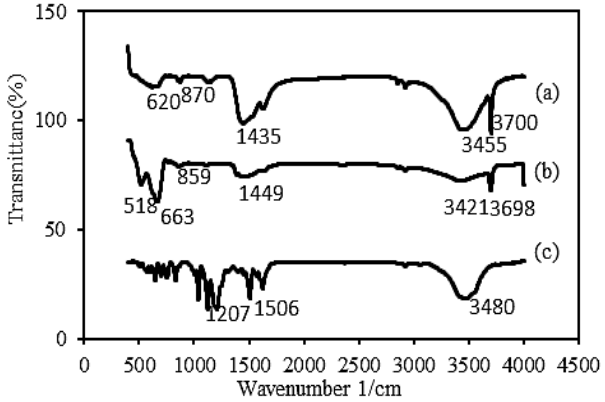

Fig. 3: IR spectra of SY/MgO (a), MgO nanoparticle (b), SY (c)

FT-IR analysis

To interpret and justify existence of SY on MgO, the IR spectrum of MgO, SY and SY coated MgO were obtained. In MgO nanoparticles (Fig. 3b), peak 3698 and peak 3421 is related to stretching bond of OH groups of due to humidity. The peak 1449 cm^{-1} is related to bending vibration of water molecule. The absorption peak in region 518 cm^{-1} is related to the Mg-O stretching vibration and regions 663 cm^{-1} to 859 cm^{-1} show Mg-O-Mg interactions (Fig. 3b) [27].

As seen in the Fig. 3c, the occurrence of the band at 3480 cm^{-1} is related to the stretching vibration of -OH group of SY dye. Apart from that, the bands which appeared at 1207 cm^{-1} and 1506 cm^{-1} belong to asymmetric stretching vibration of -SO_3 and N=N group, respectively in the dye [27]. With regard to the FT-IR spectra in (Fig. 3a), the adsorption of SY molecules on MgO nanoparticles did not move the position of peaks. Hence, the adsorption process can be based on the physical adsorption of SY without changes in its chemical structure.

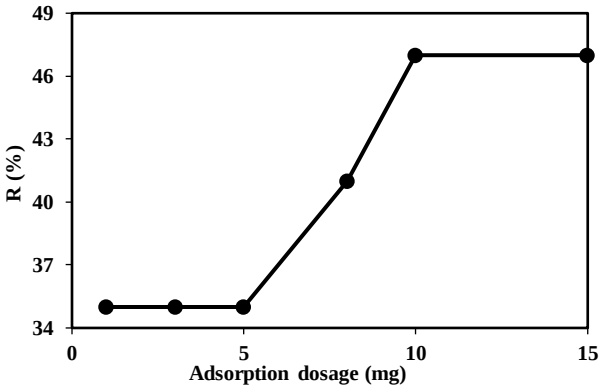

Fig. 4: Effect of adsorbent dosage on SY removal, pH= 3.0, rpm= 750, V= 10.0 mL, T= 298K, t= 20 min, C_0 =6.5 mg/L

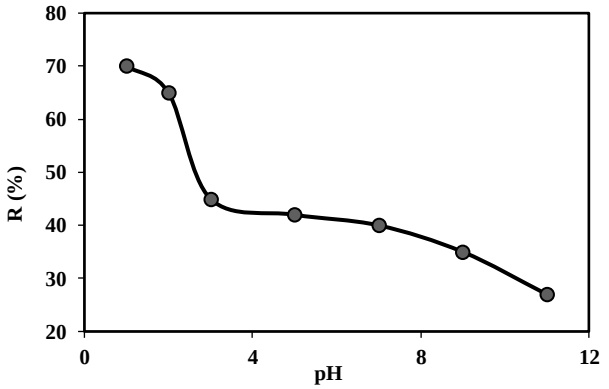

Fig. 5: Effect of pH on SY removal, adsorption dosage= 10.0 mg, rpm= 750, V= 10.0 mL, T= 298K, t= 20 min, C_0 =6.5 mg/L

Effect of different parameters

Effect of adsorbent dosage

The adsorbent amount for the adsorption studies was investigated at different values of adsorbent from 1.0 to 15.0 mg, while other parameters were kept constant. Based on these results, the SY removal increases by increasing the amount of the adsorbent and then it reached to a constant value. This observed result is due to increase in adsorption binding sites and adsorbent surface area. However, increasing the amount of adsorbent more than 10.0 mg do not demonstrate significant improvement in the removal amount of SY. This may be due to a decrease in the effective specific surface area available for metal ions resulting from the overlapping or aggregation of adsorption sites. Therefore, 10.0 mg of adsorbent was selected as the optimal amount of MgO for subsequent studies (Fig. 4).

Effect of pH

The pH solution is one of the crucial factors that affect the dye molecules' adsorption. The Fig. 5 shows the effect of pH on the SY adsorption that demonstrates adsorption, decrease from 70.0 to 27.0% at pH range of 1.0 - 11.0. The SY have two sulfonic strong acidic groups with pKa_1= 0.82 and pKa_2= 1.46 and an aza group with pKa = 9.2 [28]. On the other hand, as estimated the point of zero charge is between 11.0 and 12.0 (pH_{PZC}) for MgO nanoparticles [29]. Therefore, MgO nanoparticles are positive below 11.0. At pH 1.0 the sulfonic group was deprotonated and a negative charge is produced at SY molecule. The negative charge on the surface of dye molecules and the positive charge on the MgO surface is the reason for adsorption of SY. As the acidity of solution increased (from pH 11.0 to pH 1.0) an increasing in positive charge was occurred on MgO nanoparticles and therefore, the electrostatic attraction between MgO and SY increase. As a result, maximum adsorption of SY observes at this pH. This observation is nearly in agreement with the result obtained in literature for SY [27]. Thus, the pH=1.0 was chosen for the subsequent studies.

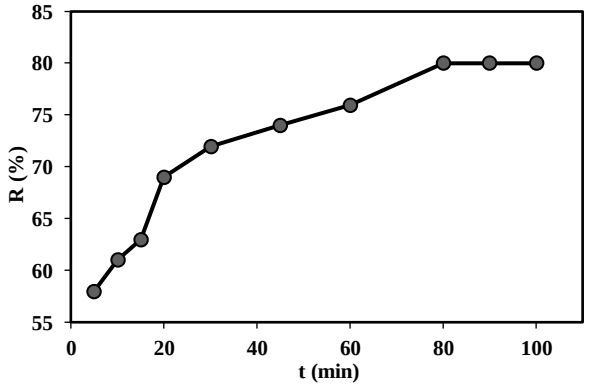

Fig. 6: Effect of contact time on SY removal adsorption dosage= 10.0 mg, pH=1.0, rpm= 750, V= 10.0 mL, T= 298 K, C_0 =6.5 mg/L

Effect of contact time

The effect of contact time on the adsorption of SY by MgO nanoparticle is illustrated in Fig. 6. The percentage of adsorption rapidly increased within the first 80.0 min, and equilibrium was achieved after 90.0 minutes of contact time. This is due to an increase in the number of adsorption sites MgO nanoparticles [30]. After this period, the adsorption efficiency was almost constant because of the adsorption sites saturated with SY dye and decrease in the diffusion rate. When this occurs, the adsorbent cannot adsorb any more dye molecules.

,

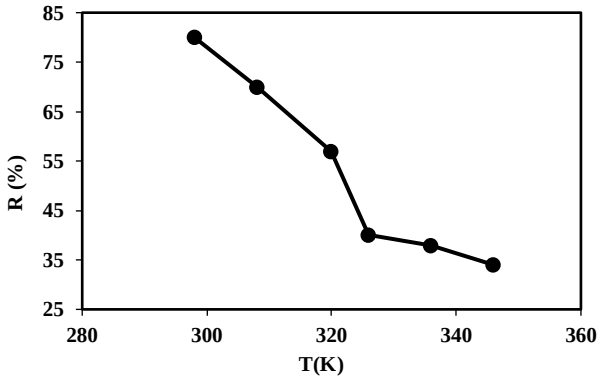

Fig. 7: Effect of temperature on SY removal adsorption dosage= 10.0 mg, and pH=1.0, t= 80 min, rpm= 750, V= 10.0 mL, C_0 =6.5 mg/L

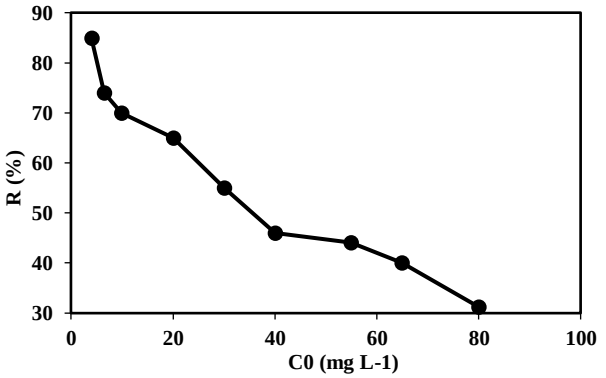

Fig. 8: Effect of initial concentration on SY removal adsorption dosage= 10.0 mg, pH=1.0, t= 80 min, rpm= 750, T= 298 K, V= 10.0 mL

Effect of temperature

The effect temperature was investigated in the temperature range of 298 -346 K. As shown in Fig. 7. with an increase in temperature, the dye removal decreased, indicating that adsorption of dye on the adsorbent was exothermic [31, 32]. An increase in temperature probably decreases the adsorption bonds between the dye molecules and the active sites on the adsorbent's surface. Therefore, the adsorption process is physical, and the lowest temperature, 298 K, is selected as the optimal temperature [33].

Effect of initial concentration of dye on the percent of removal of adsorbent

The percent removal was shown in Fig. 8. The experiments were conducted from 4.0 to 80 mg⁄L of dye. The highest percentage of removal occurs at the lowest concentration of dye. This is due to decrease in the ratio of adsorbent surface and soluble adsorption dye in concentrated solutions. Thus causes the reduction of adsorption sites and almost complete coverage of adsorption sites at high concentrations of pigment.

Thermodynamic parameters

The plot of LnK as a function of 1/T is shown in Fig. 9. The entropy ΔS° and enthalpy (ΔH°) were investigated from the intercept and slope, respectively. In addition, the calculated values of thermodynamic parameters for SY adsorption onto MgO nanoparticles are shown in Table 1. The negative ΔG° is indicated that the process of adsorption is thermodynamically favorable and spontaneous [33]. In addition, ΔG° values became positive with an increase in temperatures, showing that the process

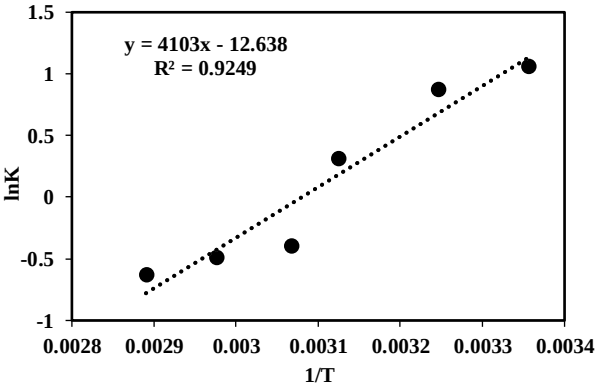

Fig. 9: The plot of LnK versus 1/T for SY adsorption dosage = 10.0 mg, t= 80 min, rpm= 750, V= 10.0 mL, pH=1.0.

of adsorption was more feasible at lower temperatures. The negative value of ΔH° revealed the exothermic behavior of the adsorption, and this result was supported by decreasing SY removal (%) with an increase in temperatures. The negative value of ΔS° illustrates a decrease in the system's randomness. As a result, there were no remarkable changes in the internal structure of MgO during the process of adsorption, which confirms the physicality of this process.

Adsorption isotherms

Langmuir isotherm and the linear curve of C_e versus C_e/q_e are shown in Fig.10a. The correlation coefficient (R^2) of this plot is 0.91, the adsorbed dye is a single layer and with the thickness of a molecule [34]. The K_L and q_{max} were calculated from the intercept and slope of linear curve, apart from that, the R_L values in Table 2, were 0.18-0.94. Therefore, these results show the favorable SY sorption under the chosen adsorption conditions.

Table 1: Values related to thermodynamic parameters for SY removal

Temperature (K)	ΔH° (kJ./mol)	ΔS° (J/(K.mol))	ΔG° (kJ.mol^{-1})
298			-2.62
308			-2.3
320	-34.11	-0.105	-0.84
326			1.06
336			1.35
346			1.8

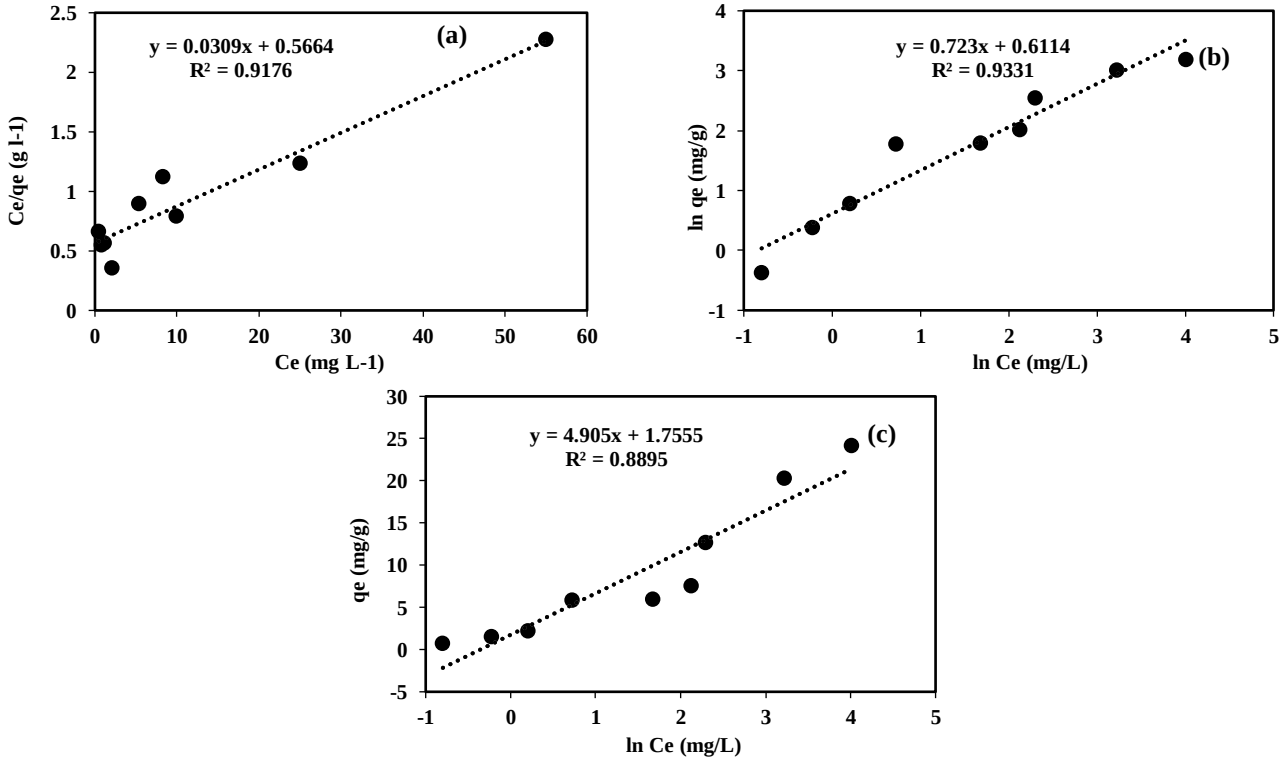

Fig. 10: (a) Langmuir, (b) Freundlich, (c) Temkin adsorption isotherms

Freundlich constants, n and K_F [35], were determined from Fig. 10b. The values of the correlation coefficient (R^2) equaled 0.93. This high value of R^2 indicates that this model is suitable for SY adsorption. K_F value was equal to 1.84. The constant n in the Freundlich isotherm indicates the intensity of adsorption. When $1 < n < 10$ indicates the favorable absorption [23, 36]. The n values for the absorption of SY were 1.38 (Table 2). This indicates a favorable adsorption process for SY adsorption driven by physical adsorption.

The plot qe as a function of ln Ce related to Temkin's equation was shown in Fig. 10c, both constants A and B (Temkin's constant) were determined from this plot. The A and B represents the equilibrium-binding constant and adsorption heat, respectively [37]. The B value was calculated 4.905 J/mg. This value indicates the physico-chemical nature of absorbent on the surface of MgO nanoparticles. The R^2 was calculated 0.88, which shows that the adsorption process was not thoroughly fitted with Temkin's isotherm model (Table 2). According to the analysis of these, three models (Freundlich, Langmuir and Temkin), the correlation coefficient value related to Freundlich isotherm was the best selection. Hence, SY adsorption gave a good fit to Freundlich's isotherm.

Adsorption kinetics

The adsorption results at different times were analyzed by well-known traditional equations like pseudo-first and

,

Table 2: ***Values related to Isometric parameters for SY adsorption***

Isotherm models	Langmuir				Freundlich			Temkin		
Parameters	q_m	k_L	R_L	R^2	n	k_F	R^2	A	B	R^2
	32.36	0.05	0.18-0.94	0.91	1.38	1.84	0.93	1.75	4.905	0.88

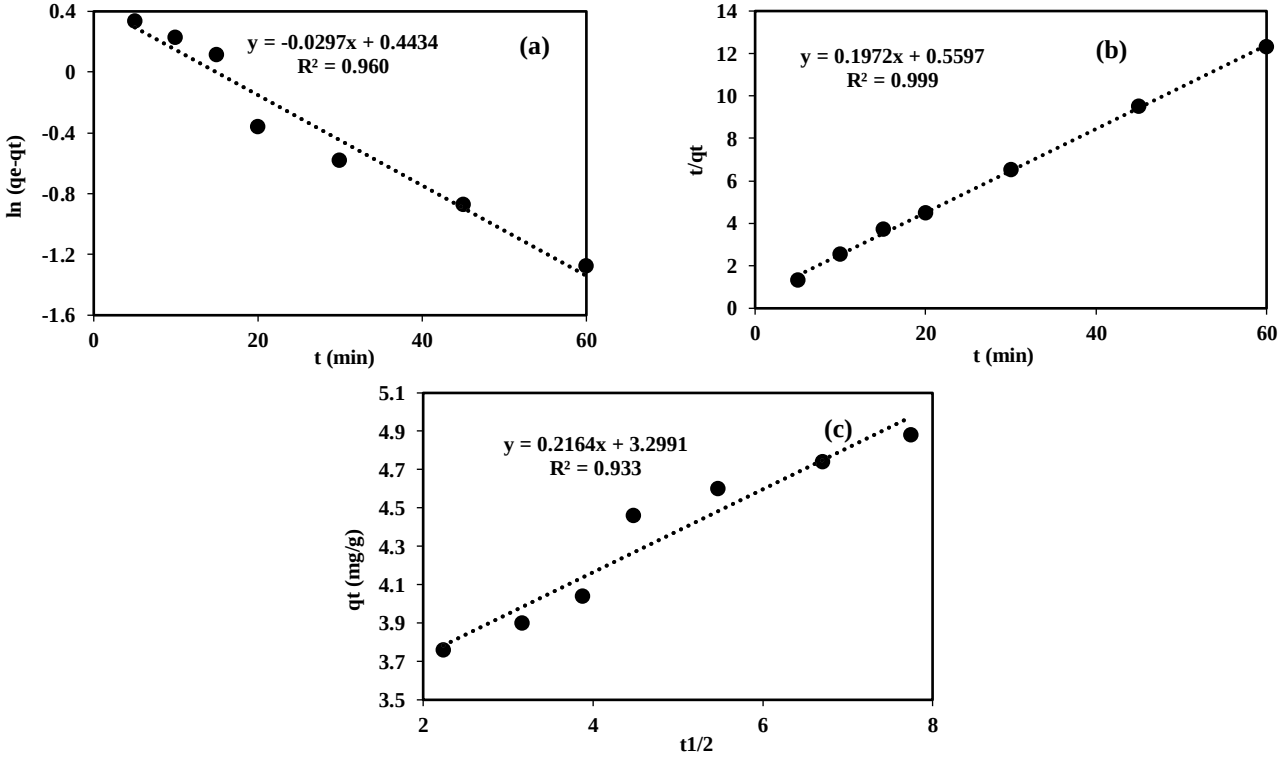

Fig. 11: (a) pseudo-first-order (b) pseudo-second- order, (c) Intra-particle diffusion adsorption kinetics.

second-order and intra-particle diffusion models. Fig. 11a and b demonstrated the plots of ln ($q_e - q_t$) and t/q_t as a function of t for the pseudo-first and pseudo-second-order reaction. In addition, the q_t plot as a function of $t^{1/2}$ was shown in Fig. 11c for the determination of the rate parameters [38]. The more fitted kinetics model was chosen based on two parameters. These parameters are first R^2 values and second qe the adsorption capacities (comparison of experimental and theoretical data). The SY adsorbent kinetic parameters are presented in Table 3. The findings showed that the R^2 value of the pseudo-second-order model is 0.99, which is better than those of pseudo-first-order (0.96), and intra-particle diffusion (0.93) models and the experimental value of q_e was in the range of (5.16 mg⁄g). The theoretical q_e was calculated based on a second-order kinetic model (5.07 mg⁄g). Consequently, the experimental data highly approved based on the pseudo-second-order model. Hence, the SY adsorption on the nanoparticle's surface was regarded as the chemisorption process and a rate-limiting step [39].

Comparison with other adsorbents

The performance of the present adsorbent has been compared with other adsorbent for the removal of SY and shown in Table 4. As can be seen the contact time for removal of the SY in some cases is better than other adsorbents. In addition, the percent of removal is not different from other adsorbents except ref of 41. Moreover, this adsorbent has some advantages such as, it is available, cheap, ecofriendly and the synthetic procedure is very simple.

COCLUSSIONS

In this study, MgO nanoparticles were effectively utilized as SY adsorbents from the aqueous medium. Based on the obtained results, 10 mg adsorbent can eliminate a high amount of SY (~85%) from the aqueous solution. The optimum condition for 85% SY removal was 80 minutes contact time, 6.5 mg⁄ L of SY and pH 1.0 at room temperature. The percentage of SY removal decreased with the increase in temperature. This is may be

Table 3: Values related to kinetic parameters for SY adsorption

Kinetics models	pseudo-first- order			pseudo-second- order			Intra-particle diffusion		
Parameters	q_e	k_1	R^2	q_e	k_2	R^2	Kp	C	R^2
	1.55	0.0297	0.96	5.07	0.069	0.99	0.216	0.329	0.93

Table 4: Comparison of the proposed method with published studies in literature for the removal of SY

Sorbent	pH	Contact time (min)	Temperature (k)	Removal (%)	Reference
Lady Finger Stem	2	30	303	75	40
Activated carbon (Wood)	1	30	298	98	41
OMC/Nd	6.5	240	298	90	42
Alligator weed activated carbon	3	240	298	90	43
MgO	1	80	298	85	This work

due to reduced adsorption forces between the dye and the nanoparticle, which justifies the physical adsorption. Based on the results of isotherms, adsorption kinetics and thermodynamics were studied in detail, and the results of the experimental data were in good agreement with the Freundlich model. To have a high R^2=0.99 value, the Freundlich model with n >1 was dominant, which justified the physical adsorption. According to kinetic analysis, it was observed that SY adsorption into MgO-fitted by the pseudo-second-order model, and thermodynamic data illustrated that since SY is spontaneous and exothermic at low temperatures, MgO can be successfully utilized to eliminate azo dye from wastewater.

Conflict of interest

We are grateful to the University of Kurdistan for its financial support (Grant No. 2018).

Received: Jan. 17, 2022 ; Accepted: May 16, 2022

References

[1] Mosallanejad N., Arami A., Kinetics and Isotherm of Sunset Yellow Dye Adsorption on Cadmium Sulfide Nanoparticle Loaded on Activated Carbon, *J. Chem. Health Risks*, **2(1):** 31–40 (2012).

[2] Alahiane S., Qourzal S., El Ouardi M., Belmouden M., Assabbane A., Ait-Ichou Y., Adsorption Et Photodégradation du Colorant Indigo Carmine En Milieu Aqueux En Présence De TiO_2/Uv/O_2, *J. Mater. Environ. Sci*., **4(2):** 239–250 (2013).

[3] Demirbas E., Kobya M., Sulak M.T., Adsorption Kinetics of a basic Dye from Aqueous Solutions onto Apricot Stone Activated Carbon, *Bioresour. Technol.*, **99(13):** 5368-5373 (2008).

[4] Kavitha D., Namasivayam C., Capacity of Activated Carbon in the Removal of Acid Brilliant Blue: Determination of Equilibrium and Kinetic Model Parameters, *Chem. Eng. J.*, **139(3):** 453-461 (2008).

[5] Ghaedi M., Shokrollahi A., Tavallali H., Shojaiepoor F., Keshavarz B., Hossainian H., Soylak M.U., Purkait M.K., Activated Carbon and Multiwalled Carbon Nanotubes as Efficient Adsorbents for Removal of Arsenazo (III) and Methyl Red from Waste Water, *Toxicol. Environ. Chem.*, **93(3):** 438-449 (2011).

[6] McKay G., Allen S.J., McConvey I.F., Otterburn M.S., Transport Processes in the Sorption of Colored Ions by Peat Particles, *J. Colloid Interface Sci.*, **80(2):** 323-339 (1981).

[7] Magdya Y.H., Altaherb H., Kinetic Analysis of the Adsorption of Dyes from High Strength Wastewater on Cement Kiln Dust, *J. Environ. Chem. Eng*., **6:** 834-841 (2018).

[8] Arabkhani P., Asfaram A., Development of a Novel Three-Dimensional Magnetic Polymer Aerogel as an Efficient Adsorbent for Malachite Green Removal, *J. hazard.mater*., **384:** 121394 (2020)

[9] Porhemmat S., Ghaedi M., Rezvani A.R., Azqhandi M.H.A., Bazrafshan A.A., Nanocomposites: Synthesis, Characterization and its Application to Removal Azo Dyes Using Ultrasonic Assisted Method: Modeling and Optimization, *Ultrason Sonochem.*, **38:** 530-543 (2017).

,

[10] Sun SC., Hsieh B.C., Chuang M.C., Electropolymerised-Hemin-Catalysed Reduction and Analysis of Tartrazine and Sunset Yellow, *Electrochim. Acta.*, **319:** 766-774 (2019).

[11] Song Y., Liu Y., Chen S., Qin H., Xu H., Carmine Adsorption From Aqueous Solution by Crosslinked Peanut Husk, *Iran. J. Chem. Chem. Eng. (IJCCE)*, **33(4):** 69-77 (2014).

[12] Ahmad Z.U., Yao L., Wang J., Gang D.D., Islam F., Lian Q., Zappi M.E., Neodymium Embedded Ordered Mesoporous Carbon (OMC) for Enhanced Adsorption of Sunset Yellow: Characterizations, Adsorption Study and Adsorption Mechanism, *Chem. Eng. J.*, **359:** 814-826 (2019).

[13] Aghaie-Khouzani M., Forootanfar H., Moshfegh M., Khoshayand M.R., Faramarzi M.A., Variable, *Biochem. Eng. J.*, **60:** 9-15 (2012).

[14] Tünay O., Kabdasli I., Eremektar G., Orhon D., Color Removal from Textile Wastewaters, *Water Sci.Technol.*, **34(11):** 9-16 (1996).

[15] Roosta M., Ghaedi M., Daneshfar A., Darafarin S., Sahraei R., Purkait M.K., Simultaneous Ultrasound-Assisted Removal of Sunset Yellow and Erythrosine by ZnS: Ni Nanoparticles Loaded on Activated Carbon: Optimization by Central Composite Design, *Ultrason. Sonochem.*, **21(4):** 1441-1450(2014).

[16] Hassan M.S., El-Nemr K.F., Dye Sorption Characters of Gamma Irradiated Foamed Ethylene Propylene Diene Monomer (EPDM) Rubber/Clay Composites, *J.Ind. Eng. Chem.*, **19(4):** 1371-1376 (2013).

[17] Khayatian G., Jodan M., Hassanpoor S., Mohebbi S., Determination of Trace Amounts of Cadmium, Copper and Nickel in Environmental Water and Food Samples Using GO/MgO Nanocomposite as a New Sorbent, *J. Iran. Chem. Soc.*, **13:** 831-839 (2016).

[18] Askari P., Faraji A., Khayatian G., Mohebbi S., Effective Ultrasound-Assisted Removal of Heavy Metal Ions As (III), Hg (II), and Pb (II) from Aqueous Solution by New MgO/CuO and MgO/MnO_2 Nanocomposites, *J. Iran. Chem. Soc.*, **14:** 613-621 (2017).

[19] Karthik K., Dhanuskodi S., Gobinath C., Prabukumar S., Sivaramakrishnan S., Fabrication of MgO Nanostructures and its Efficient Photocatalytic, Antibacterial and Anticancer Performance, *J. Photochem. Photobiol., B*, **190:** 8-20 (2019).

[20] Yao C., Pan Y., Lu H., Wu P., Meng Y., Cao X., Xue S., Utilization of Recovered Nitrogen from Hydrothermal Carbonization Process by Arthrospira Platensis, *Bioresour. Technol.*, **212:** 26-34 (2016).

[21] Lima E.C., Hosseini-Bandegharaei A., Moreno-Piraján JC., Anastopoulos I., A Critical Review of the Estimation of the Thermodynamic Parameters on Adsorption Equilibria. Wrong use of Equilibrium Constant in the Van't Hoof Equation for Calculation of Thermodynamic Parameters of Adsorption, *J. Mol. Liq.*, **273:** 425-434 (2019).

[22] Samiee Beyragh A., Varsei M., Meshkini M., Khodadadi Darban A., Gholami E., Kinetics and Adsorption Isotherms Study of Cyanide Removal from Gold Processing Wastewater using Natural and Impregnated Zeolites, *Iran. J. Chem. Chem. Eng. (IJCCE)*, **37(2):** 139-149 (2018).

[23] Ahmad M.A., Alrozi R., Removal of Malachite Green Dye from Aqueous Solution using Rambutan Peel-Based Activated Carbon: Equilibrium, Kinetic and Thermodynamic Studies, *Chem. Eng.*, **171(2):** 510-516 (2011).

[24] Xu H., Liu D.-d., He L., Liu N., Ning G., Adsorption of Copper (II) from a Wastewater Effluent of Electroplating Industry by Poly (ethylenediamine)-Functionalized Silica, *Iran. J. Chem. Chem. Eng. (IJCCE)*, **34(2):** 73-81 (2015).

[25] Zadvarzi S.B., Khavarpour M., Vahdat S.M., Baghbanian S.M., Rad A.S., Synthesis of Fe3O4@ Chitosan@ ZIF-8 Towards Removal of Malachite Green from Aqueous Solution: Theoretical and Experimental Studies, *In. J. Bio. Mac.*, **168:** 428-441 (2021).

[26] Luo T., Liang H., Chen D., Ma Y., Yang W., Highly Enhanced Adsorption of Methyl Blue on Weakly Cross-Linked Ammonium-Functionalized Hollow Polymer Particles, *Appl. Surf. Sci.*, **505:** 144607 (2020).

[27] Yayayürük O., Yayayürük A.E., Özmen P., Karagöz B., PDMAEMA Grafted Microspheres as an Efficient Adsorbent for the Removal of Sunset Yellow from Pharmaceutical Preparations, Beverages and Waste Water, *Eur. Polym. J.*, **141:** 110089 (2020).

[28] Gomez M., Arancibia V., Rojas C., Nagles E., Adsorptive Stripping Voltammetric Determination of Tartrazine and Sunset Yellow in Gelatins and Soft Drink Powder in the Presence of Cetylpyridinium Bromide, *Int. J. Electrochem. Sci.*, **7:** 7493-7502 (2012).

[29] Díez R., Medina O.E., Giraldo L.J., Cortés F.B., Franco C.A., Development of Nanofluids for the Inhibition of Formation Damage Caused by Fines Migration: Effect of the Interaction of Quaternary Amine (CTAB) and MgO Nanoparticles, *Nanomaterials*., **10:** 928 (2020).

[30] Mouni L., Belkhiri L., Bollinger J.C., Bouzaza A., Assadi A., Tirri A., Dahmoune F., Madani K., Remini H., Removal of Methylene Blue from Aqueous Solutions by Adsorption on Kaolin: Kinetic and Equilibrium Studies, *Appl. Clay. Sci.*, **153:** 38-45 (2018).

[31] Banerjee S., Sharma G.C., Gautam R.K., Chattopadhyaya M.C., Upadhyay S.N., Sharma Y.C., Removal of Malachite Green, a Hazardous Dye from Aqueous Solutions using Avena Sativa (oat) Hull as a Potential Adsorbent, *J. Mol. Liq.*, **213:** 162-172 (2016).

[32] Ofomaja A.E., Ho Y.S., Equilibrium Sorption of Anionic Dye from Aqueous Solution by Palm Kernel Fibre as Sorbent, *Dyes. Pigms.*, **74(1):** 60-66 (2007).

[33] Lima E.C., Hosseini-Bandegharaei A., Moreno-Piraján J.C., Anastopoulos I., A Critical Review of the Estimation of the Thermodynamic Parameters on Adsorption Equilibria. Wrong use of Equilibrium Constant in the Van't Hoof Equation for Calculation of Thermodynamic Parameters of Adsorption, *J. Mol. Liq.*, **273:** 425-434 (2019).

[34] Binaeian E., Seghatoleslami N., Chaichi M.J., Synthesis of Oak Gall Tannin-Immobilized Hexagonal Mesoporous Silicate (OGT-HMS) as a New Super Adsorbent for the Removal of Anionic Dye from Aqueous Solution, *Desalination. Water. Treat.*, **57(18):** 8420-8436 (2016).

[35] Bhattacharyya K.G., Sharma A., Kinetics and Thermodynamics of Methylene Blue Adsorption on Neem (Azadirachta Indica) Leaf Powder, *Dyes Pigms.*, **65(1):** 51-59 (2005).

[36] Rozada F., Calvo L.F., Garcıa A.I., Martın-Villacorta J., Otero M., Dye Adsorption by Sewage Sludge-based Activated Carbons in Batch and Fixed-Bed Systems, *Bioresour. Technol.*, **87(3):** 221-230 (2003).

[37] Bayramoglu G., Yilmaz M., Azo Dye Removal using Free and Immobilized Fungal Biomasses: Isotherms, Kinetics and Thermodynamic Studies, *Fibers and Polymers.*, **19(4):** 877-886 (2018).

[38] Yamini Y., Faraji M., Rajabi A.A., Nourmohammadian F., Ultra Efficient Removal of Basic Blue 41 from Textile Industry's Wastewaters by Sodium Dodecyl Sulphate Coated Magnetite Nanoparticles: Removal, Kinetic and Isotherm Study, *Anal and Bioanal. Chem. Res.*, **5(2):** 205-215 (2018).

[39] Sharifpour E., Khafri H.Z., Ghaedi M., Asfaram A., Jannesar R., Isotherms and Kinetic Study of Ultrasound-Assisted Adsorption of Malachite Green and Pb^{2+} Ions from Aqueous Samples by Copper Sulfide Nanorods Loaded on Activated Carbon: Experimental Design Optimization, *Ultrason. Sonochem.*, **40:** 373-382 (2018).

[40] Abbas A., Rehman R., Murtaza S., Shafique U., Zahid A., Ayub R., Adsorptive Removal of Congo Red and Sunset Yellow Dyes from Water Systems by Lady Finger Stem, *J. Chem. Soc.*, **34(5):** 1241-1246 (2012).

[41] Ghaedi AM., Ghaedi M., Karami P., Comparison of Ultrasonic with Stirrer Performance for Removal of Sunset Yellow (SY) by Activated Carbon Prepared from Wood of Orange Tree: Artificial Neural Network Modeling, *Spectrochimica Acta Part A: Mol. Biomol. Spectrosc.*, 138: 789-799 (2015).

[42] Ahmad ZU., Yao L., Wang J., Gang D.D., Islam F., Lian Q., Zappi M.E., Neodymium Embedded Ordered Mesoporous Carbon (OMC) for Enhanced Adsorption of Sunset Yellow: Characterizations, Adsorption Study and Adsorption Mechanism, *Chem. Eng. J.*, **359:** 814-826 (2019).

[43] Kong Q., Liu Q., Miao MS., Liu Y.Z., Chen Q.F., Zhao C.S., Kinetic and Equilibrium Studies of the Biosorption of Sunset Yellow Dye by Alligator Weed Activated Carbon, *Desalination. Water. Treat.*, **66:** 281-290 (2017).